

EFFECT OF REACTION CONDITIONS ON PARTICLE SIZE OF ZNO NANOPARTICLES VIA CONTROLLED PRECIPITATION METHOD AND IN-VITRO ANTIBACTERIAL CAPACITY**Miguel A. Pedroza Toscano^a, Rodolfo Salazar Peña^a, Martín Rabelero Velasco^b, José J. Ibarra Montalvo^c, Jesús A. Aréchiga Guzmán^c and Susana López Cuenca^{c,*}**^aDepartamento de Investigación, Centro Universitario UTEG, 44430, Guadalajara Jalisco, México^bDepartamento de Ingeniería Química, CUCEI, Universidad de Guadalajara, 44430, Guadalajara Jalisco, México^cInstituto Tecnológico José Mario Molina Pasquel y Henríquez unidad académica Zapopan, 45019, Zapopan Jalisco, México

Recebido em 10/01/2022; aceito em 15/02/2022; publicado na web em 24/03/2022

High-yield ZnO spheroidal nanoparticles with an average diameter around 23 nm ($\approx 25\%$ frequency) and 30 nm ($\approx 28\%$ frequency) were obtained by controlled semicontinuous precipitation at low temperatures. This synthesis was obtained from hydrozincite ($\text{Zn}_5(\text{CO}_3)_2(\text{OH})_6$) as primary nanoparticles. The $\text{Zn}_5(\text{CO}_3)_2(\text{OH})_6$ nanoparticles were synthesized by hydrolysis of $\text{Zn}(\text{NO}_3)_2$ in aqueous solution of $(\text{NH}_4)_2\text{CO}_3$ and later, the precipitation becomes. Two temperatures of 60 and 70 °C in combination with three times of reaction were tested; followed by calcination of the precipitate at 400 °C. This range of sizes of nanoparticles is comparable with those obtained by other methods reported in the literature, such as microemulsions, however, here the advantage was not using solvents or surfactants. The ZnO nanoparticles were characterized by energy dispersive X-ray spectroscopy coupled to a scanning electron microscopy (SEM-EDS), transmission electronic microscopy (TEM), and X-ray diffraction. The antibacterial activity of the films against Gram-positive (*S. aureus*) and Gram-negative (*E. coli.*) bacteria was investigated using the disc diffusion method. The best results were found in the inhibition zone for Gram-positive bacteria, when the concentration of ZnO NPs incorporated was 3 mg disc⁻¹.

Keywords: nanomaterials; particle size; high production; characterization methods; antimicrobial; semicontinuous precipitation.

INTRODUCTION

The modern era of nanotechnology began to unfold in the nineteen-eighties. Since then, a part of the scientific community studies the synthesis, behavior, and application of nanostructural material.¹ This interest is due to the size particle-physics properties caused by spatial changes in energy levels, besides the ratio area-volume obtained by the small size of the particles.²

Nowadays, nanoparticles of zinc oxide (ZnO) are among the most considered in research, mostly by their ratio of economical cost versus all high versatility in applications. For instance, these are used in the primary component of material in piezoelectronics,³ sensors,⁴ photovoltaic cells,⁵ antibacterial items,⁶ deodorants,⁷ photocatalytic activity,^{8,9} etc. Moreover, zinc oxide is a biocompatible material, making it suitable in medical applications. This depending on the size of the particles and on their morphology.¹⁰ Some studies are devoted to investigating the effect of zinc oxide NPs in cancer treatments.¹¹ Jiang *et al.*¹² report that, thanks to their antibacterial effects and their effectiveness on some treatments against diabetes, promising results are arising in the field of health sciences. Given this scope, there are strenuous research looking for novel methods on the synthesis for these NPs that allow the sizing control on the resulting product.¹³

There are several methods to obtain nanoparticles. As follows, we mention some of them that stand out, these are: colloidal methods,^{14,15} hydrothermal treatment,^{15,16} the use of organometallic compounds,¹⁷ sol-gel,^{18,19} sonochemical synthesis,²⁰ microwaving,²¹ green synthesis,^{22,23} etc. In our consideration, one of the most outstanding of these methods is the semicontinuous precipitation. That because, it is profitable, since expensive equipment is not needed.²⁴ Moreover, chemical reactions for synthesis are carried at relatively low temperatures, i.e., below 90 °C. This contrasts with hydrothermal and solvothermic methods in which synthesis reactions

are carried out at high temperatures and pressures. On the other hand, avoiding the use of organic solvents makes a feasible environmentally friendly production. Organic solvents are necessary in sol-gel and microemulsions methods. Furthermore, it is worth noting that the method here presented, does not need the addition of capping agents or surfactants to obtain small particles. These are an essential quality for their use as antimicrobial and antifungal agent.²⁵

In this contribution, the method of synthesis for zinc oxide nanoparticles by semicontinuous precipitation was tested. The regarded variables that likely affect the resulting nanoparticles size were the effect of the addition time of the precipitating agent and the temperature on the reactive process. The material obtained was characterized by SEM-EDS, XRD, TEM and the antibacterial effect was tested as well.

EXPERIMENTAL

The following chemical substances were used: Hexahydrate zinc nitrate ($\text{Zn}(\text{NO}_3)_2 \cdot 6\text{H}_2\text{O}$) 98% pure, Ammonium carbonate ($(\text{NH}_4)_2\text{CO}_3$), 99.99% pure, Acetone (CH_3COCH_3) 99.5% pure from Sigma-Aldrich, were used as received, and de-ionized and triple-distilled water with conductivity smaller than 6 $\mu\text{S cm}^{-1}$.

The synthesis of the ZnO NPs was carried out in a pair of replicas using the bifactorial experimentation. The corresponding design is shown in Table 1. A 24% w/w solution of ammonium carbonate was added as precipitating agent (pH=7.62). The reaction was carried out by addition of 75 mL of 0.90 mol L⁻¹ zinc nitrate solution (pH=4.43). This solution was used as a precursor agent for the ZnO NPs. The reactive system consists in a magnetically stirred 250 mL three-necked flask with controlled temperature into a range of 60 to 70 °C. Then, ammonium carbonate solution, was dosed as reductor agent of the zinc oxide nanoparticles. This process was performed at different feeding rates, i.e., 0.27, 0.22 and 0.18 g min⁻¹, this with the aim of to give total feeding times of 100, 125, and 150 min respectively. After periods,

*e-mail: susana.lopez@zapopan.tecmm.edu.mx

the reacting system was left to stand for 30 min at the same reaction temperature. The molar ammonium carbonate/zinc nitrate ratio was 10% higher than the stoichiometric ratio; the final pH was 5.5.

Table 1. Bifactorial experimental design for ZnO NPs production

Sample	Temperature (°C)	Reaction Time (min)
100-1	60	100
125-1	60	125
150-1	60	150
100-2	70	100
125-2	70	125
150-2	70	150

The precipitated was recovered by filtration and washed with an aqueous acetone solution (81/19 w / w). Then, it was located into an ultrasonic bath for 15 minutes. In this way, it was possible to eliminate the remaining substances of the reaction. This procedure was repeated five times. The residual wet solid was dried in an oven at 60 °C for 24 h. Previous works reported that the particle size may depends on the calcination temperature of the primary material. According to Raoufi,²⁶ the higher calcination temperature, the larger the particle size. Therefore, it was decided to calcine in an oven at 400 °C for about two hours. The samples were labeled by the addition time, being number 1 for the precipitation at 60 °C and 2 for 70 °C.

The presence of ZnO NPs in the powder after the purification procedure was determined by energy-dispersive X-ray spectroscopy coupled to a scanning electron microscopy (SEM-EDS) from Tescan, model MIRA 3 LMU-Bruker. The soft white powder as resulted product, was characterized by XRD in an Empyrean diffractometer (PANalytical) scanning into a range of 10 to 80 2θ degrees. The particle size was determined by transmission electronic microscopy (TEM) in a JEOL JEM- 1010. For this purpose, the resulting powder was dispersed in acetone with an ultrasonicator. A drop of the dispersion was located on a copper grid, where the solvent was allowed to evaporate at room temperature. TEM images of the nanoparticles were used for the size distribution measurements. Over two hundred particles were measured to obtain the particle average size as well their size distribution. The particle average crystallite sizes were obtained by using the Scherrer equation:

$$d = \frac{K\lambda}{\beta \cos\theta} \quad (1)$$

Being d the average crystallite size in nm, K the dimensional factor (0.9), λ the X-ray wavelength (0.154 nm), β the line broadening at half the maximum intensity in radians, and θ the Bragg's angle.

The purity of the final product was determined by atomic absorption spectrometry (Varian Spectra 250 AA).

The nanoparticles synthesized were tested for antibacterial activity by agar disk diffusion method against the Gram-positive pathogenic bacteria *Staphylococcus aureus* (ATCC 25923) and Gram-negative *Escherichia coli* (ATCC 25922). The bacterial isolates were cultured on nutrient broth at 37 °C. Following incubation, a standard inoculum of each bacterial isolate was prepared to a concentration of 10^7 CFU mL⁻¹ and compared with a 0.5 McFarland standard solution. An inoculum volume of 0.15 mL of each strain was spread homogeneously onto the individual agar plates using sterile cotton swabs. Sterile filter paper disc (6 mm diameter) impregnated by three different ZnO-NPs concentration (1, 2, 3 mg disc⁻¹), were placed on the nutrient agar plates on which bacteria were spread. The plates were incubated at 37 °C for 24 h; after incubation, the presence of inhibition zones was measured. For each bacterial strain, three replicas were performed. The minimal

inhibitory concentration (MIC) was evaluated for the ZnO NPs, as described Ghanbari and Salavati-Niasari.²⁷

RESULTS AND DISCUSSION

EDS Analysis

To verify the presence and purity of the material obtained, the technique SEM-EDS was used. For instance, Figure 1 shows a Photograph from SEM of sample 100-2 described in Table 1, on which agglomerated particles can be seen. A specific area from the observed surface was selected to apply EDS analysis, obtaining components and composition from it. The EDS spectrum is shown in Figure 2 where signals for zinc and oxygen representative of the ZnO were found. The presence of carbon can be attributed to carbon adhesive tape. All samples were analyzed following the same methodology and similar results were obtained in all cases, where intense signals are observed at 1 and 8.7 keV confirming the presence of ZnO. Table 2 shows the EDS analysis of all the samples studied, where we can highlight that the atomic percentage for Zn and O is one by one, which is why it is concluded that the material obtained is ZnO.

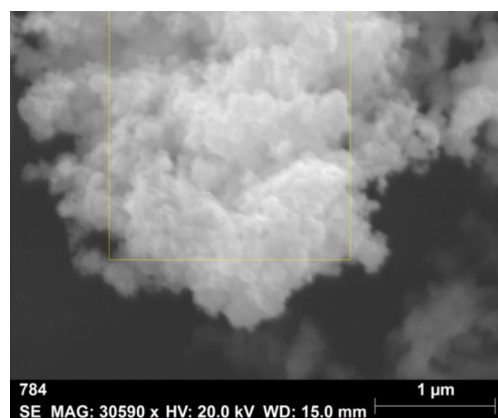


Figure 1. SEM image obtained from purified ultrafine powder

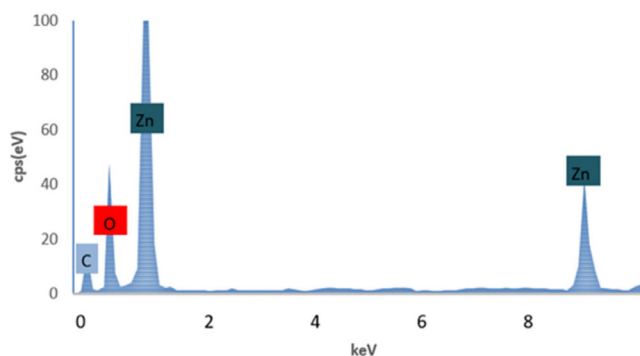


Figure 2. EDS spectra of zinc oxide nanoparticles

X-Ray diffraction pattern

Figure 3 shows the X-ray diffraction pattern (XRDP) of the ZnO NPs precursor. The XRDP of the precursor material shows the major characteristic signals of the hydrozincite (ICDD no. 00-019 – 1458). In the figure, the peaks fit with the standard. Similar XRD spectra were obtained for all the samples. The precipitation reaction was carried out according to the chemical reaction:

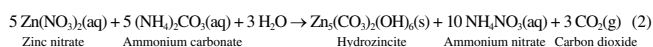


Table 2. EDS analysis for each treatment

Sample	Element	Weight%	Atomic%
100-1	O K	19.66	49.99
	Zn K	80.4	50.01
125-1	O K	20.28	50.97
	Zn K	79.72	49.03
150-1	O K	19.66	49.99
	Zn K	80.34	50.01
100-2	O K	20.42	51.19
	Zn K	79.58	48.81
125-2	O K	19.65	49.99
	Zn K	80.35	50.01
150-2	O K	19.67	50.01
	Zn K	80.33	49.99

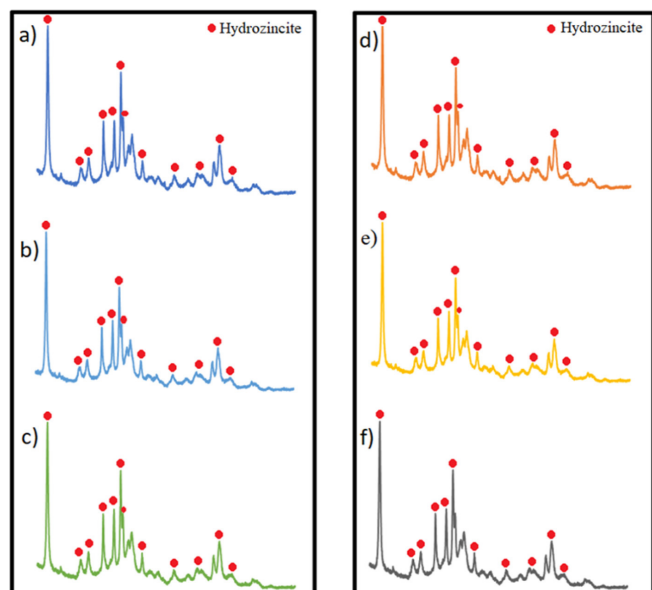
**Figure 3.** X-ray diffraction patterns for all samples. a) 100-1, b) 125-1, c) 150-1, d) 100-2, e) 125-2, f) 150-2

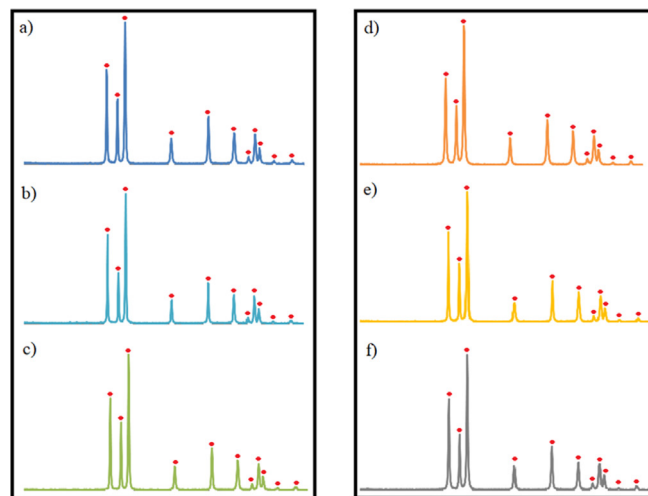
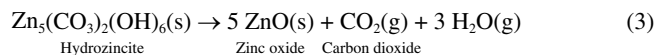
Table 3 shows the crystallite size of precursor nanoparticles obtained with Scherrer equation. The crystallite size was on the range of 12.66 – 17.45 nm.

Table 3. Crystallite size of hydrozincite particles

Sample	Crystallite Size (nm)
100-1	15.88
125-1	16.35
150-1	17.45
100-2	11.37
125-2	12.66
150-2	13.27

Figure 4 shows the x-ray patterns obtained for ZnO nanoparticles and its standard (ICDD no. 00-036-1451). In the figure, the peaks fit with the standard. The crystallographic arrangement was hexagonal, i.e., wurzita according to this standard. All samples have similar diffraction patterns. Table 4 shows the average diameters of the ZnO NPs calculated using the Scherrer equation into the range of 22.49 – 27.93 nm.

The reaction that was caused by the calcination of the precursor material is:

**Figure 4.** X-ray diffraction patterns for all samples. a) 100-1, b) 125-1, c) 150-1, d) 100-2, e) 125-2, f) 150-2

TEM analysis

Figure 5 shows the micrograph taken of the ZnO particles and their histogram obtained from the particle diameter of sample 100-2. We can highlight that the particles are agglomerated, as other authors have reported.²⁸ The structure of ZnO nanoparticles is spheroidal according to micrographs with diameters less than 40 nm. Table 4 shows the results obtained from the characterization of ZnO nanoparticles, as we foresight and as it is observed, the higher the temperature, the smaller particle diameter obtained. This agrees with that reported in the literature such as Gusatti *et al.*,²⁹ that is, the crystallite size for the samples made with a temperature of 50 °C is greater than for those carried out at a temperature of 90 °C. In addition, the morphology obtained at $t \leq 70$ °C is nanorod and at higher temperatures the morphology is spheroidal. On the other hand, Chandrasekaran *et al.*³⁰ found the same temperature correlation with particle size, finding that the particle size was 76.46 nm when the reaction temperature was 100 °C, a size larger than that found by Gusatti *et al.*,²⁹ when the synthesis was carried out at 90 °C (28 nm). López-Cuenca *et al.*³¹ also report this same phenomenon, but conclude that the correlation between particle size and reaction temperature was not statistically significant.³¹ The correlation between particle size and temperature is due to the fact that the nucleation rate is strongly related to the reaction temperature, being faster at higher temperatures the higher the nucleation rate, the smaller the size particle.³² The authors above mentioned, used zinc nitrate as a precursor agent and sodium hydroxide was used as the precipitating agent. In this work, it is highlighted that the particle sizes of NPs are smaller than those reported when precipitating agents is NaOH.

In general, for this synthesis of nanoparticles, these particle sizes are smaller than others reported in the literature under similar reaction conditions, where sizes are around 35.2 nm.³³ We attribute these obtained sizes to the method of the reaction that was carried out. In our case, the precipitating agent was added and not the precursor, thus, favoring a high $\text{Zn}^{2+}/\text{CO}_3^{2-}$ ratio. This increases considerably the nucleation speed and therefore decreasing the aggregation speed due to the high competition between them and the low availability of surrounding Zn^{2+} ions. These effects result in slow growth and small sizes. Otherwise, where the precursor agent is added, the $\text{Zn}^{2+}/\text{CO}_3^{2-}$ ratio is lower, causing the creation of few nucleation

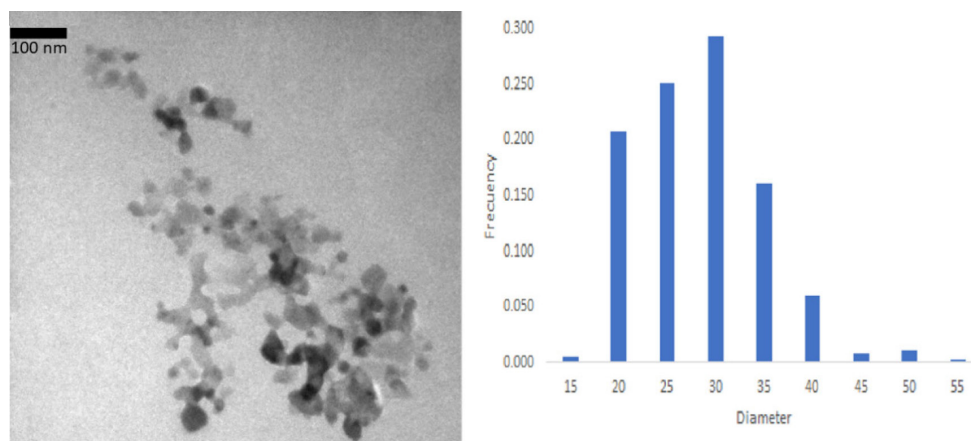


Figure 5. Micrographs of the zinc oxide and histogram of nanoparticles obtained for sample 100-2

centers. These grow rapidly when interacting with the high availability of surrounding Zn^{2+} ions, so the aggregation speed is higher creating larger crystals.

Also, it is observed, that the longer the reaction time, the slightly increase the particle size. This is because the increasing the reaction time. The rate of addition of the precipitating agent decreases, resulting in a lower nucleation rate and an increase in the particle sizes.³²

Additionally, this method allowed us to use a molar concentration of 0.9 in zinc nitrate, thus allowing a high yield of Zn nanoparticles, when molar concentrations are usually reported in the literature below 0.06 mol L^{-1} ²⁸ to be able to achieve the same particle sizes.

Table 4. shows atomic absorption analysis exhibited that the nanoparticles have a high purity (ZnO, 96-99%), in addition to the high yields obtained by gravimetric analysis.

Antibacterial activity of zinc oxide nanoparticles

The result revealed that ZnO-NPs have antibacterial activity against both tested bacterial strains. The nanoparticles exhibited a maximum inhibition zone for 3 mg disk^{-1} of 11.9 mm and 14.1 mm for *E. coli* and *S. aureus* respectively. This is consistent with previously

reported results.³⁴⁻³⁶ Figure 6 shows the zones of inhibition for sample 5 (all the samples exhibit similar inhibition zone).

Figure 7 shows the average zone of inhibition for all samples for three replicates. The minimum inhibitory concentration (MIC) of ZnO-NPs against *S. aureus* and *E. coli* was less than $0.13 \text{ mg disk}^{-1}$ bactericidal activity showed greater susceptibility to *S. aureus* than to *E. coli*. This is probably due to the different structures of the cell membrane of both bacteria. In addition, the cell wall of Gram-negative cells (*E. coli*) is wavy and double-layered, with a lipopolysaccharide membrane.³⁷

CONCLUSIONS

Spheroidal ZnO-NPs with hexagonal structure were obtained by semicontinuous controlled precipitation method and calcinate. This method resulted to be an easy, low cost, synthesis under low temperature and environment-friendly. With this process, ZnO nanoparticles from 20 to 31 nm of high purity and with hexagonal wurtzite structure were synthesized. The characterizations carried out by XRD and TEM demonstrated the obtaining of spheroidal ZnO-NPs synthesized at a temperature lower (60 and $70 \text{ }^\circ\text{C}$) with a molar concentration of 0.9 in

Table 4. Particle size and ZnO content for each treatment

Sample	Crystallite Size (nm)	Dn (nm)	PDI	ZnO ^a purity (%)	Yield ^b (%)
100-1	23.60	23.45 ± 3.12	1.18	92	95.12
125-1	25.75	25.97 ± 6.40	1.19	92	95.4
150-1	27.93	30.31 ± 5.31	1.1	98	89.44
100-2	22.49	22.67 ± 5.45	1.21	87	91.84
125-2	25.07	25.95 ± 6.41	1.18	95	93.2
150-2	25.92	27.14 ± 6.85	1.17	90	92.8

^aCalculated from atomic absorption determinations. ^b(Experimental weight of ZnO/theoretical weight of ZnO) \times 100.

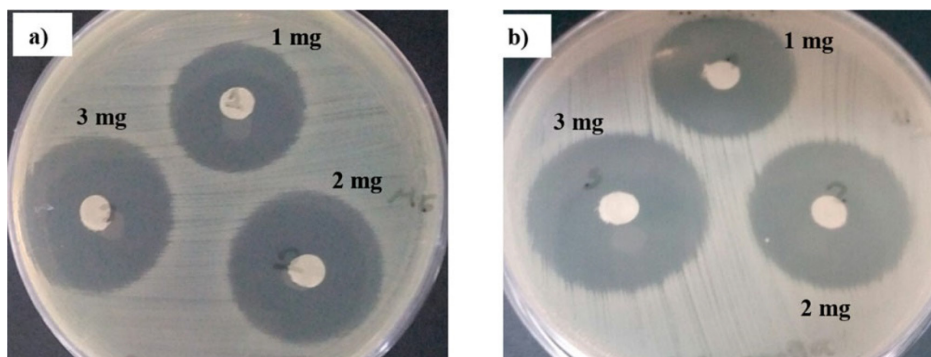


Figure 6. Inhibition zone for a) *E. coli* b) *S. aureus*

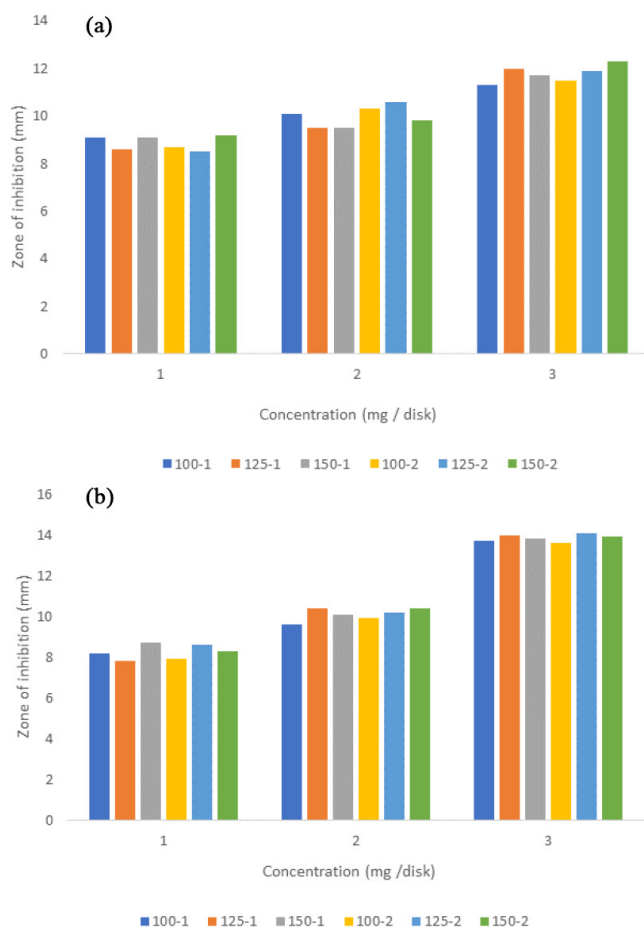


Figure 7. Inhibition zone (mm) of the ZnO NPs in-situ against all tested bacterial strains for a) *E. coli* b) *S. aureus*

zinc nitrate, allowing a high performance of the nanoparticles. It was observed, that when the rate of addition is decreased the particle size increases. As well as the lower the temperature, the larger the particle size. The ZnO-NPs showed an antimicrobial effect for both bacteria and antibacterial activity observed was similar to the nanoparticles obtained by other processes. *S. aureus* and *E. coli*, were inhibited by ZnO-NPs. However, *S. aureus* was more susceptible than *E. coli*. In general, these results open a situation for future research using concentrations and temperatures higher than those used in this research, which could improve the production per reaction batch, since it is one of the limitations in all the methods of synthesis of nanoparticles.

REFERENCES

- Hulla, J. E.; Sahu, S. C.; Hayes, A. W.; *Hum. Exp. Toxicol.* **2015**, *34*, 1318.
- Guisbiers, G.; Mejia-Rosales, S.; Deepak, F. L.; *J. Nanomater.* **2012**, 180976.
- Rahman, W.; Garain, S.; Sultana, A.; Ranjan Middy, T.; Mandal, D.; *Mater. Today* **2018**, *5*, 9826.
- Pan, Y.; Zuo, J.; Hou, Z.; Huang, Y.; Huang, C.; *Front. Chem.* **2020**, *8*, 592538.
- Wibowo, A.; Marsudi, M. A.; Amal, M. I.; Ananda, M. B.; Stephanie, R.; Ardy, H.; Diguna, L. J.; *RSC Adv.* **2020**, *10*, 42838.
- Petkova, P.; Francesco, A.; Perelshtein, I.; Gedanken, A.; Tzanov, T.; *Ultrason. Sonochem.* **2016**, *29*, 244.
- Hall-Puzio, P.; Gale, A.; Brahm, J.; *U. S. pat. US20010031248A1* **2001**.
- Martínez-Vargasa, B. L.; Díaz-Realá, J. A.; Reyes-Vidalá, Y.; Rodríguez-

- López, J. L.; Ortega-Borgesá, R.; Ortiz-Frade, L.; *Quim. Nova* **2017**, *40*, 6.
- Alshams, H. A. A.; Al-Bedairy, M. A.; Alwan, S. H.; *IOP Conference Series: Earth and Environmental Science* **2021**, *722*, 012005.
- Deák, G.; Dumitru, F. D.; Moncea, M. A.; Panait, A. M.; Baraitaru, A. G.; Olteanu, M. V.; Boboc, M. G.; Stanciu, S.; *Int. J. Conserv. Sci.* **2019**, *10*, 343.
- Barui, A. K.; Kotcherlakota, R.; Patra, C. R.; *Inorganic Frameworks as Smart Nanomedicines*, 1st ed., William Andrew Publishing: Norwich, 2018.
- Wang, J.; Lee, J. S.; Kim, D.; Zhu, L.; *ACS Appl. Mater. Interfaces.* **2017**, *9*, 39971.
- Jiang, J.; Pi, J.; Cai, J.; *J. Nanomater.* **2018**, 1062562.
- Dakhlaoui, A.; Jendoubi, M.; Smiri, L. S.; Kanaev, A.; Jouini, N.; *J. Cryst. Growth.* **2009**, *311*, 3989.
- Alshamsi, H. A. H.; Hussein, B. S.; *Orient. J. Chem.* **2018**, *34*, 1898.
- Winkelmann, M.; Schuler, T.; Uzunogullari, P.; Winkler, C. A.; Gerlinger, W.; Sachweh, B.; Schuchmann, H. P.; *Chem. Eng. Sci.* **2013**, *81*, 209.
- Ojha, D. P.; Kim, H. J.; *Chem. Eng. Sci.* **2019**, *212*, 115338.
- Ryzhikov, A.; Jońca, J.; Kahn, M.; Fajrwerger, K.; Chaudret, B.; Chapelle Ménini, P.; Shim, C. H.; Gaudon, A.; Fau, P.; *J. Nanopart. Res.* **2015**, *17*, 280.
- Al-Bedairy, M. A.; Alshamsi, H. A. H.; *Eurasian J. Anal. Chem.* **2018**, *13*, em72.
- Noman, M. T.; Petru, M.; Militký, J.; Azeem, M.; Ashraf, M. A.; *Materials* **2019**, *13*, 14.
- Hasanpoor, M.; Aliofkhaezae, M.; Delavari, H.; *Procedia Mat. Sci.* **2015**, *11*, 320.
- Pillai, A. M.; Sivasankarapillai, V. S.; Rahdar, A.; Joseph, J.; Sadeghfar, F.; Anuf, A. R.; Rajesh, K.; Kyzas, G. Z.; *J. Mol. Struct.* **2020**, *1211*, 8 pages.
- Irshad, S.; Salamat, A.; Anjum, A. A.; Sana, S.; Saleem, R. S.; Naheed, A.; Iqbal, A.; *Cogent Chem.* **2018**, *4*, 1469207.
- Pedroza-Toscano, M. A.; López-Cuenca, S.; Moreno-Medrano, E. D.; Rabelero-Velasco, M.; Salazar-Peña, R.; *Micro Nano Lett.* **2018**, *13*, 951.
- Padalia, H.; Chanda, S. *Artif. Cells Nanomed. Biotechnol.* **2017**, *45*, 1751.
- Raoufi, D.; *J. Lumin.* **2013**, *134*, 213.
- Ghanbari, M.; Salavati-Niasari, M.; *Ecotoxicol. Environ. Saf.* **2021**, *208*, 111712.
- An, L. J.; Wang, J.; Zhang, T. F.; Yang, H. L.; Sun, Z. H.; *Adv. Mat. Res.* **2011**, *380*, 335.
- Gusatti, M.; Sousa, D. A.; Durazzo, M.; Riella, H. G. In *Manufacturing Nanostructures*; Wagar, A., Nasar, A., eds.; One Central Press: Manchester, 2014, p. 50.
- Romadhan, M. F.; Suyatma, N. E.; Taqi, F. M.; *Indones. J. Chem.* **2016**, *16*, 117.
- López-Cuenca, S.; Aguilar-Martínez, J.; Rabelero-Velasco, M.; Hernández-Ibarra, F. J.; López-Ureta, L. C.; Pedroza-Toscano, M. A.; *Rev. Mex. Ing. Quim.* **2019**, *18*, 1179.
- Shevchenko, E. V.; Talapin, D. V.; Schnablegger, H.; Kornowski, A.; Festin, Ö.; Svedlindh, P.; Weller, H.; *J. Am. Chem. Soc.* **2003**, *125*, 9090.
- Chen, C.; Liu, P.; Lu, C.; *Chem. Eng. J.* **2008**, *144*, 509.
- Padmavathy, N.; Vijayaraghavan, R.; *STAM* **2008**, *9*, 035004.
- Raunak, S.; Subramani, K.; Petchi, M. R.; Rangaraj, S.; Venkatachalam, R.; *Prog. Org. Coat.* **2018**, *124*, 80.
- Mohammad, A. A.; Mahadevamurthy, M.; Daruka, P.; Ahmad, Almatroudi.; *Biomolecules* **2020**, *10*, 336.
- Talodthaisong, C.; Plaeyao, K.; Mongseetong, C.; Boonta, W.; Srichaiyapol, O.; Patramanon, R.; Kayunkid, N.; Kulchat, S.; *Nanomaterials* **2020**, *11*, 442.

